Feshbach resonances in ultracold mixtures of the fermionic quantum gases 6Li and 40K

Tiecke, T.G.

Publication date
2009

Chapter 5
Asymptotic Bound-state Model

In this chapter we present an Asymptotic Bound-state Model which can be used to accurately describe all Feshbach resonance positions and widths in a two-body system. With this model we determine the coupled bound states of a particular two-body system. The model is based on analytic properties of the two-body Hamiltonian, and on asymptotic properties of uncoupled bound states in the interaction potentials. In its most simple version, the only necessary parameters are the least bound state energies and actual potentials are not used. The complexity of the model can be stepwise increased by introducing threshold effects, multiple vibrational levels and additional potential parameters. The model is extensively tested on the ^{6}Li-^{40}K system and additional calculations on the ^{40}K-^{87}Rb and ^{3}He* - ^{4}He* systems are presented.
This chapter will be submitted to Physical Review A. Parts of the model have been published in Ref. [18] and in Ref. [17] Physical Review Letters **100** 053201 (2008)

5.1 Introduction

The field of ultracold atomic gases has been rapidly growing during the past decades. One of the main sources of growth is the large degree of tunability to employ ultracold gases as model quantum systems [95, 174]. In particular the strength of the two-body interaction parameter, captured by the scattering-length a, can be tuned over many orders of magnitude. A quantum system can be made repulsive ($a > 0$), attractive ($a < 0$), non-interacting ($a = 0$) or strongly interacting ($|a| \to \infty$) in a continuous manner by means of Feshbach resonances. Feshbach resonances are induced by external fields: magnetically induced Feshbach resonances are conveniently used for alkali-metal atoms, while optically induced Feshbach resonances seem more promising for e.g. alkaline-earth atoms [62]. In this paper we consider magnetically induced resonances only.
Feshbach resonances depend crucially on the existence of an internal atomic structure, which can be modified by external fields. For alkali-metal atoms, this structure is initiated by the hyperfine interaction, which can be energetically modified by a magnetic field via the Zeeman interaction. For a given initial spin state, its collision threshold and its two-body bound states depend in general differently on the magnetic field. A Feshbach resonance occurs when the threshold becomes degenerate with a bound state. Accurate knowledge of the Feshbach resonance structure is crucial for experiments
The two-body system has to be solved to obtain the bound state solutions. Since the interactions have both orbital and spin degrees of freedom, this results in a set of radially coupled Schrödinger equations in the spin basis. The set of equations is referred to as Coupled Channels equations [175], and can be solved numerically. Quite often it is

far from trivial to obtain reliable predictions for the two-body problem, due to several reasons: the ab-initio interaction potentials are usually not accurate enough to describe ultracold collisions. Therefore these potentials have to be modelled by adding and modifying potential parameters. A full calculation for all spin combinations and all potential variations is very time-consuming. Moreover, one can easily overlook some features of the bound state spectrum due to numerical issues such as grid sizes and numerical accuracy. This is also due to a lack of insight of the general resonance structure, which is often not obvious from the numerical results.

Given the above, there is certainly a need for fast and simple models to predict and describe Feshbach resonances, which allow for a detailed insight in the resonance structure. In the last decade various simple models have been developed for ultracold collisions [47, 176, 177], which vary significantly in terms of complexity, accuracy and applicability. In all these models the radial equation plays a central role in finding the Feshbach resonances. In this paper we present in detail the Asymptotic Bound-state Model (ABM). This model, briefly introduced in Ref. [17], was successfully applied to the Fermi-Fermi mixture of ^{6}Li and ^{40}K. Here the observed loss features where assigned to 13 Feshbach resonances with high accuracy, and the obtained parameters served as an input to a full coupled channels analysis. The ABM builds on an earlier model by Moerdijk et al. [82] for homonuclear systems, which was also applied by Stan et al. [178] for heteronuclear systems. This model neglects the mixing of singlet and triplet states, therefore allowing the use of uncoupled orbital and spin states. In ABM we make use of the radial singlet and triplet eigenstates and include the coupling between them. This crucial improvement makes the whole approach in principle exact, and it allows for a high degree of accuracy given a limited number of parameters.

We show how we can systematically extend the most simple version of ABM to predict the width of the Feshbach resonances by including threshold behavior. Additionally we allow for the inclusion of multiple vibrational levels and parameter for the spatial wavefunction overlap. The fact that ABM is computationally light provides the possibility to map out the available Feshbach resonance positions and widths for a certain system, as has been shown in [18]. Throughout the paper we will use the ^{6}Li-^{40}K mixture as a model system to illustrate all introduced aspects. Additionally, we present ABM calculations on the ^{40}K-^{87}Rb mixture to demonstrate its validity on a more complex system, comparing it with accurate coupled channel calculations [179]. Finally, we make predictions for Feshbach resonances in the heteronuclear metastable helium (^{3}He*-^{4}He*) mixture.

In the following we describe the ABM model (Sec. 5.2) and various methods to obtain the required input parameters. In Sec. 5.3 the ABM is applied to the three physical systems and in Sec. 5.4 we introduce the coupling to the open channel to predict the width of Feshbach resonances. In section 5.5 we summarize our findings and comment on further extensions of the model.

5.2 Asymptotic Bound-state Model

We assume that the two colliding atoms both are initially prepared in a hyperfine state $|fm_f\rangle$, where f is the total spin and m_f its projection along the magnetic field axis. The two-body tensor product formed by the hyperfine states of the two atoms is called the *entrance channel*. To predict the position of a Feshbach resonance we calculate the energy

of the entrance channel and that of a coupled bound state as a function of the magnetic field. We expect Feshbach resonances at magnetic field values where the entrance channel energy equals the energy of the molecular state. In this section we will show how the ABM can be used to determine the energy of the entrance channel and of the coupled bound states.
The effective Hamiltonian describing the collision of two ground-state alkali atoms in the center of mass frame is given by [12]

$$\mathcal{H} = \frac{\mathbf{p}^2}{2\mu} + \mathcal{H}^{\text{int}} + \mathcal{V}, \tag{5.1}$$

where the first term is the relative kinetic energy with μ the reduced mass, $\mathcal{H}^{\text{int}}$ the internal energy of the two atoms and $\mathcal{V}$ the effective interaction between the atoms. We use the *bound* eigenstates $|\psi_\sigma\rangle$ of the relative Hamiltonian $\mathcal{H}^{\text{rel}} = \frac{\mathbf{p}^2}{2\mu} + \mathcal{V}$ as a basis for the secular equation

$$\det\left|(\epsilon_\sigma - E)\delta_{\sigma,\sigma'} + \left\langle\psi_\sigma\left|\mathcal{H}^{\text{int}}\right|\psi_{\sigma'}\right\rangle\right| = 0, \tag{5.2}$$

where the eigenvalues ϵ_σ are the binding energies of the uncoupled bound states of the relative Hamiltonian and σ is a label for all orbital and spin degrees of freedom. The solutions of the secular equation yield the energies of the coupled bound states as a function of magnetic field. Next we will specify the internal degrees of freedom of the two atoms, followed by a more detailed discussion of the relative Hamiltonian, the free parameters of the model and a description of asymptotic bound states.

5.2.1 Internal energy

The single atom internal Hamiltonian consists of hyperfine and Zeeman interactions

$$\mathcal{H}^{\text{hf}} = \frac{a_{\text{hf}}}{\hbar^2}\mathbf{i}\cdot\mathbf{s} + (\gamma_e\mathbf{s} - \gamma_i\mathbf{i})\cdot\mathbf{B}, \tag{5.3}$$

where $\mathbf{s}$ and $\mathbf{i}$ are the electron and nuclear spins respectively, γ_e and γ_i are their respective gyromagnetic ratios, a_{hf} is the hyperfine energy and $\mathbf{B}$ is the externally applied magnetic field. The hyperfine interaction couples the electron and nuclear spin which add to a total angular momentum $\mathbf{f} = \mathbf{s} + \mathbf{i}$. In Fig. 5.1 the well known hyperfine diagrams of ^{6}Li and ^{40}K are shown, the curves correspond to the eigenvalues of $\mathcal{H}^{\text{hf}}$. The one-atom hyperfine states are labeled $|fm_f\rangle$, although f is only a good quantum number in the absence of an external magnetic field. By labelling the colliding atoms with α and β, the interaction process can be described in the basis of the two-body internal states $|f_\alpha m_{f_\alpha}, f_\beta m_{f_\beta}\rangle$.
Since the effective interactions $\mathcal{V}$ can be neglected asymptotically, the threshold energy for two interacting atoms is completely determined by the two-body internal Hamiltonian $\mathcal{H}^{\text{int}} = \mathcal{H}^{\text{hf}}_\alpha + \mathcal{H}^{\text{hf}}_\beta$. Consequently, the threshold energy (E_{thr}) for a certain spin configuration (i.e. entrance channel) is the sum of the single atom internal energies. For a certain total energy E the threshold energy determines if a channel is open ($E > E_{\text{thr}}$) or closed ($E > E_{\text{thr}}$).

5.2.2 Relative Hamiltonian

The bound eigenstates of $\mathcal{H}^{\text{rel}}$ are crucial to determine the coupled bound states responsible for the Feshbach resonances. The relative Hamiltonian consists of effective interactions

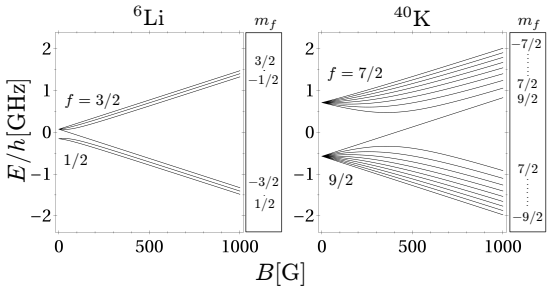

Figure 5.1: The single atom hyperfine diagrams for ^{6}Li and ^{40}K. The curves correspond to the eigenvalues of $\mathcal{H}^{\rm hf}$ and are labeled by the zero field quantum numbers $|fm_f\rangle$.

$\mathcal{V}$ resulting from all Coulomb interactions between the nuclei and electrons of both atoms [1]. These central interactions depend only on the quantum number S associated with the magnitude of the total electron spin $\mathbf{S} = \mathbf{s}_\alpha + \mathbf{s}_\beta$, therefore they can be decomposed as $\mathcal{V} = \sum_S |S\rangle \mathrm{V}_S \langle S|$ where the potential V_S is either the singlet ($S = 0$) or triplet ($S = 1$) potential. Note that for central interactions the two-body solutions will depend on orbital quantum number l, but not on its projection m_l. Both these quantum numbers are conserved.

We specify the ABM basis states $|\psi_\sigma\rangle$ as $|\psi_S^{\nu,l}\rangle|Sm_S\mu_\alpha\mu_\beta\rangle$. Here we define the spin basis states $|Sm_S\mu_\alpha\mu_\beta\rangle$ via spin quantum number S and the magnetic quantum numbers m_S, μ_α, and μ_β of the $\mathbf{S}$, $\mathbf{i}_\alpha$ and $\mathbf{i}_\beta$ operators respectively. The sum $m_F = m_S + \mu_\alpha + \mu_\beta$ is conserved, therefore limiting the number of spin states involved. The bound states for the singlet and triplet potentials, characterized by the vibrational and orbital quantum numbers ν and l, satisfy the eigenvalue equation for the relative motion, where we projected $\mathcal{H}^{\rm rel}$ on a specific S and l state:

$$\left[-\frac{\hbar^2}{2\mu}\frac{d^2}{dr^2} + V_S^l(r)\right]\psi_S^{\nu,l}(r) = \epsilon_S^{\nu,l}\psi_S^{\nu,l}(r). \tag{5.4}$$

Here $\psi_S^{\nu,l}(r) = \langle r|\psi_S^{\nu,l}\rangle$ is the relative reduced wavefunction, r the interatomic separation, and $V_S^l(r) \equiv l(l+1)\hbar^2/(2\mu r^2) + V_S(r)$. The corresponding binding energies are given by $\epsilon_S^{\nu,l}$. In this paper we focus on heteronuclear systems, however, the ABM works equally well for homonuclear systems. In the latter case one would rather use a symmetrized spin basis $|Sm_sIm_I\rangle$, where I is the total nuclear spin and m_I is the magnetic quantum number for $\mathbf{I}$ as described in Ref. [82].

Now that we have defined a complete basis, the internal Hamiltonian can be written as $\mathcal{H}_{\rm int} = \mathcal{H}_{\rm int}^+ + \mathcal{H}_{\rm int}^-$, where the $\mathcal{H}_{\rm int}^+$ part gives rise to hyperfine coupling within the separate singlet and triplet subspaces, while $\mathcal{H}_{\rm int}^-$ takes care of the coupling between the singlet and triplet manifolds. The latter term was neglected in the models of Refs. [82, 178].

For central interactions the orbital angular momentum is conserved, therefore we can solve Eq. (5.2) separately for every l-subspace:

[1] The much weaker magnetic dipole-dipole interactions are neglected.

$$\det|_{\nu,l}\langle Sm_S\mu_\alpha\mu_\beta|\left(\epsilon_S^{\nu,l}+\mathcal{H}_{\rm int}^{+}-E\right)\delta_{\nu,\nu'} \\ +\eta_{S,S'}^{\nu,\nu'}\mathcal{H}_{\rm int}^{-}|S'm'_S\mu'_\alpha\mu'_\beta\rangle_{\nu',l}|=0. \tag{5.5}$$

Here $\eta_{S,S'}^{\nu,\nu'}=\langle\psi_S^{\nu,l}|\psi_{S'}^{\nu',l}\rangle$ is the Franck-Condon factor which value generally is in the range $0\leq|\eta_{S,S'}^{\nu,\nu'}|\leq 1$, while only bound states within the same potential $V_S^l(r)$ are exactly orthonormal: $\langle\psi_S^{\nu,l}|\psi_S^{\nu',l}\rangle=\delta_{\nu,\nu'}$.

5.2.3 Free parameters

The free parameters of the ABM are the binding energies $\epsilon_S^{\nu,l}$ and the Franck-Condon factors $\eta_{S,S'}^{\nu,\nu'}$ describing the relative motion. These parameters can be obtained in a variety of manners. Here we discuss three methods which will be demonstrated in Sect. 5.3.
First, if the scattering potentials $V_S^l(r)$ are very well known, the bound state wavefunctions of the vibrational levels can be obtained by solving equation (5.4) for $\epsilon_S^{\nu,l}<0$. Numerical values of the Franck-Condon factors follow from the obtained eigenstates. This method is very accurate and can be extended to deeply bound levels, however accurate model potentials are only available for a limited number of systems.
A second method to obtain the free parameters is useful when the potentials are not very well or only partially known. For large interatomic distances the potentials can be parameterized by the asymptotically correct dispersion potential

$$V(r)=-\frac{C_6}{r^6}, \tag{5.6}$$

however, at short range this expression is no longer correct. Therefore we account for the inaccurate inner part of the potential by a boundary condition based on the accumulated phase method [86]. This boundary condition has a one-to-one relationship to the interspecies s-wave singlet and triplet scattering lengths. This method would then require only three input parameters: the van der Waals C_6 coefficient and the singlet (a_S) and triplet (a_T) scattering lengths. For an accurate description involving deeper bound states the accumulated phase boundary condition needs more parameters than only a scattering length.
The last method to obtain the free parameters is by comparing predicted positions of Feshbach resonances directly to experimental cold collision data, for instance by comparing it to atom loss. A loss feature spectrum can be obtained by holding an ultracold sample for a given time period at a particular magnetic field. The binding energies and Franck-Condon factors are obtained by fitting the calculated threshold crossings,which are the positions of the Feshbach resonances to the loss features. We used this method in Ref. [17], where it has proven to be very powerful due to the small computational time required to solve the eigenvalue equation.
The number of fit parameters is determined by the number of bound states which have to be considered. Depending on the atomic species and the magnetic field, a selected number of vibrational levels $\epsilon_S^{\nu,l}$ have to be taken into account. This number can be estimated by considering the maximum energy range involved. An upper bound results from comparing the maximum dissociation energy of the least bound vibrational level D^*

with the maximum internal energy of the atom pair $E_{\mathrm{int,max}}$. Using the dissociation energy of the N_ν-th vibrational level from [180] we obtain:

$$N_\nu \simeq \zeta \frac{\sqrt{\mu} C_6^{1/6}}{h} E_{\mathrm{int,max}}^{1/3} \tag{5.7}$$

where h is Planck's constant and ζ is a numerical constant. $E_{\mathrm{int,max}}$ is given by the sum of four terms; the hyperfine splitting of each of the two atoms at zero field, the maximum Zeeman energy for the free atom pair and the maximum Zeeman energy for the molecule. The constant ζ can be evaluated semi classically, yielding $\zeta = 1.8294$ [180], or numerically using the accumulated phase method, yielding $\zeta = 1.643$, in the following we will use the latter.

5.2.4 Asymptotic bound states

The most crucial parameters for ABM are the binding energies $\epsilon_S^{\nu,l}$, however, for accurate predictions of the Feshbach resonance positions, one also needs a rather accurate value for the Franck-Condon factors. For weakly bound states these factors are mainly determined by the binding energy difference between the bound states, rather than the potential shape. Therefore good approximations can be made with little knowledge of the scattering potential. For bound states with $r_c \gg r_0$, where r_c is the classical turning point and

$$r_0 = \frac{1}{2}\left(\frac{2\mu C_6}{\hbar^2}\right)^{1/4} \tag{5.8}$$

is the van der Waals range of the interaction potential, most of the probability density is at internuclear distances where the potential shape is unimportant. These bound states are commonly denoted as *halo states* [181]. The wavefunction is well described by $\psi(r) \sim e^{-\kappa r}$, where $\kappa = \sqrt{-2\mu\epsilon/\hbar^2}$ is the wavevector corresponding to a bound state with binding energy ϵ. The Franck-Condon factor of two weakly bound states with wavevectors κ_0 and κ_1 is given by

$$\langle \psi_0 | \psi_1 \rangle = \frac{2\sqrt{\kappa_0 \kappa_1}}{\kappa_0 + \kappa_1}. \tag{5.9}$$

This approximation is valid for states with $r_c \gg r_0$, i.e., for binding energies of $|\epsilon| \ll C_6/r_0^6$. The calculation of the Franck-Condon factors can be extended to deeper bound states by including the dispersive van der Waals tail. For $r \gg r_X$ where r_X is the radius where the van der Waals interaction equals the exchange interaction, the potential is well described by $-C_6/r^6$.The Franck-Condon factors can be calculated by numerically solving the Schrödinger equation (5.4) in the $-C_6/r^6$ potential for $r_X < r < \infty$ [182]. This method can be used for much deeper bound states, where $r_c \gg r_X$. We will define *asymptotic bound states* as states for which $r_c > r_X$. If even deeper bound states, with $r_c < r_X$, have to be taken into account, the potential can be extended by including the exchange interaction [79], or by using full model potentials.

To illustrate the validity of describing Feshbach resonances by asymptotic bound states we calculate the Franck-Condon factor for a contact potential (halo states), a van der Waals potential (asymptotic bound states) and a full model potential including short range behavior. Figure 5.2 shows the Franck-Condon factor η_{01}^{11} for ^{6}Li-^{40}K calculated numerically for the model potential, van der Waals potential, and analytically using equation (5.9).

The van der Waals coefficient used is $C_6 = 2322 E_h a_0^6$, where $E_h = 4.35974 \times 10^{-18}$J and $a_0 = 0.05291772$nm [183]. The η_{01}^{11} has been plotted as a function of the triplet binding energy ϵ_1 for three different values of the singlet binding energy ϵ_0. It is clear that the contact potential is only applicable for $\epsilon/h \lesssim 100$MHz, hence only for systems with resonant scattering in the singlet and triplet channels. The approximation based on the C_6 potential yields good agreement down to binding energies of $\epsilon \lesssim h \times 40$GHz, which is much more than the maximum possible vibrational level splitting of the least bound states ($D^* = h \times 8.2$GHz). The black circle indicates the actual Franck-Condon factor for the least bound state of ^{6}Li-^{40}K. For the contact, van der Waals and model potentials we find $\eta_{01}^{11} = 0.991$, $\eta_{01}^{11} = 0.981$ and $\eta_{01}^{11} = 0.979$ respectively.

5.3 Application to various systems

In this section we demonstrate the versatility of the ABM by applying it to three different systems using the three different approaches as discussed in Sect. 5.2.3.

5.3.1 ^{6}Li$-^{40}$K

Both ^{6}Li and ^{40}K have electron spin $s = 1/2$, therefore the total electron spin can be singlet $S = 0$ or triplet $S = 1$. We intend to describe all loss features observed in Ref. [17]. Since all these features where observed for magnetic fields below 300G we find that, by use of Eq. (5.7), it is sufficient to take only the least bound state ($\nu = 1$) of the singlet and triplet potential into account. This reduces the number of fit parameters to $\epsilon_1^{0,l}$ and $\epsilon_1^{1,l}$. Subsequently, we parameterize the $l > 0$ bound state energies by making use of model potentials as described by [184, 46] [2]. This allows us to reduce the number of binding energies to be considered to only two: $\epsilon_0^{1,0} \equiv \epsilon_0$ and $\epsilon_1^{1,0} \equiv \epsilon_1$. We now turn to the Franck-Condon factor η_{01}^{11} of the two bound states. As discussed in Sect. 5.2.4 its value is $\eta_{01}^{11} = 0.979$ and can be taken along in the calculation or approximated as unity. We first consider the case of $\eta_{01}^{11} \equiv 1$, this reduces the total number of fit parameters to only two. We fit the positions of the threshold crossings to the 13 observed loss features reported in Ref. [17] by minimizing the χ^2 value while varying ϵ_0 and ϵ_1. We obtain optimal values of $\epsilon_0/h = 716(15)$MHz and $\epsilon_1/h = 425(5)$MHz, where the error bars indicate one standard deviation. In Fig. 5.3, the threshold and spectrum of coupled bound states with $m_F = +3(-3)$ is shown for positive (negative) magnetic field values. The color scheme indicates the admixture of singlet and triplet contributions in the bound states. Feshbach resonances will occur at magnetic fields where the energy of the coupled bound state and the scattering threshold match. The strong admixture of singlet and triplet contributions at the threshold crossings emphasizes the importance of including the singlet-triplet mixing term $\mathcal{H}_{\rm int}^-$ in the Hamiltonian. All 13 calculated resonance positions have good agreement with the coupled channel calculations as described in Ref. [17], verifying that the ABM yields a good description of the threshold behavior of the ^{6}Li$-^{40}$K system for the studied field values.
We repeat the χ^2 fitting procedure now including the numerical value of the overlap. The η_{01}^{11} for both the s-wave and p-wave bound states are calculated numerically while varying

[2] Note that this procedure can also be applied with only a C_6 coefficient by utilizing the accumulated phase method

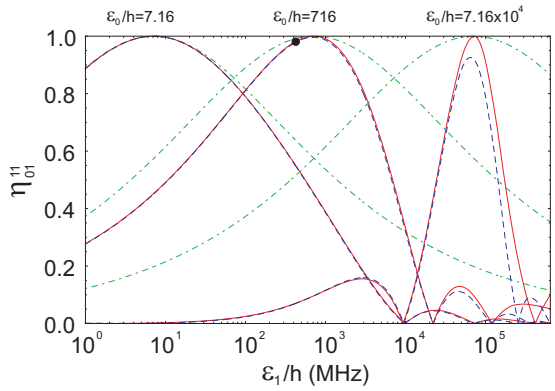

Figure 5.2: The Franck-Condon factor η_{01}^{11} for the ^{6}Li-^{40}K system calculated as a function of the triplet binding energy ϵ_1 for three different values of $\epsilon_0/h = 7.16$ MHz, $\epsilon_0/h = 716$ MHz and $\epsilon_0/h = 7.16 \times 10^4$ MHz. η_{01}^{11} is calculated for a model potential (dashed blue), a $-C_6/r^6$ potential (solid red) and a contact potential, equation (5.9) (dash-dotted green). The black circle indicates the actual value for the least bound state of ^{6}Li-^{40}K ($\epsilon_0/h =$ 716MHz and $\epsilon_1/h = 425$MHz). The nodes in η_{01}^{11} correspond to deeper lying vibrational states.

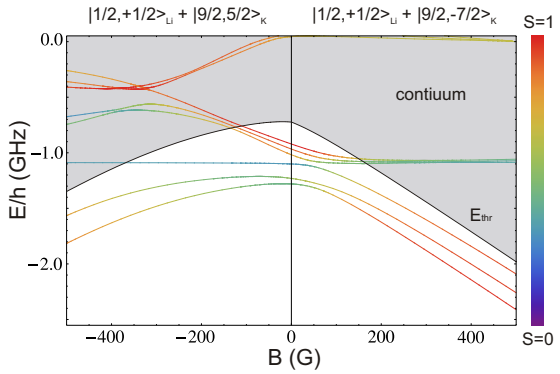

Figure 5.3: Here we have calculated the energies of all the coupled bound states for ^{6}Li-^{40}K with total spin $m_F = \pm 3$. The black solid line indicates the threshold energy of the entrance channel $|\{1/2, +1/2\}_{\mathrm{Li}}; \{9/2, +5/2\}_{\mathrm{K}}\rangle$ for $B < 0$ and $|\{1/2, +1/2\}_{\mathrm{Li}}; \{9/2, -7/2\}_{\mathrm{K}}\rangle$ for $B > 0$. The grey area represents the scattering continuum and the (colored) lines indicate the coupled bound states. Feshbach resonances occur when a bound state crosses the threshold energy. The color scheme indicates the admixture of singlet and triplet contributions in the bound states. The strong admixture near the threshold crossings at $B \simeq 150G$ demonstrate the importance of the singlet-triplet mixing in describing Feshbach resonance positions accurately. Since in the ABM the coupled bound states are not coupled to the entrance channel, they exist even for $E > E_{thr}$.

ϵ_0 and ϵ_1. This fit results in a slightly larger χ^2 value with corresponding increased discrepancies in the resonance positions. However, all of the calculated resonance positions are within the experimental widths of the loss features. Therefore, the analysis with $\eta_{01}^{11} \equiv 1$ and $\eta_{01}^{11} = 0.979$ can be safely considered to yield the same results within the experimental accuracy.

5.3.2 ^{40}K-^{87}Rb

We now turn to the ^{40}K-^{87}Rb mixture to demonstrate the application of the ABM model to a system including multiple vibrational levels and multiple non-trivial values for the overlap. Although accurate K-Rb scattering potentials are known [185], we choose to use the accumulated phase method as discussed in Sect. 5.2.3 using only three input parameters to demonstrate the accuracy of the ABM for a complex system like ^{40}K-^{87}Rb. We solve the radial Schrödinger equation (5.4) for $V_S^l(r) = -C_6/r^6$ and $\epsilon_S^{\nu,l} = \hbar^2 k^2/2\mu$ where $k \to 0$. We obtain the accumulated phase at $r_{in} = 18a_0$ by imposing a boundary condition at $r \to \infty$ using the s-wave phase shift $\delta_0 = \arctan(-ka)$, where a the s-wave scattering length. Subsequently we obtain binding energies for the three last bound states of the singlet and triplet potential by solving the same equation (5.4) but now with the accumulated phase at $r = r_{in}$ and $\psi(r \to \infty) = 0$ as boundary conditions. We numerically calculate the Franck-Condon factors by normalizing the wavefunctions for $r > r_{in}$, thereby neglecting the part of the wavefunction in the inner part of the potential ($r < r_{in}$). This assumption becomes less valid for more deeply bound states. We use as input parameters $C_6 = 4274 E_h a_0^6$ [183], $a_S = -111.5a_0$ and $a_T = -215.6a_0$ [185]. Figure 5.4 shows the spectrum of bound states with respect to the threshold energy for the mixture of ^{40}K $|f = 9/2, m_f = -9/2>$ and ^{87}Rb $|f = 1, m_f = +1>$ states. The red curves indicate the result of the ABM model and the blue curves are full coupled channel calculations [186]. The agreement between the two models is satisfactory, especially for the weakest bound states close to the threshold. The large negative scattering lengths indicates the presence of virtual bound states in both the singlet and triplet potentials. However, taking only the bound states into account already yields a good result. A conceptually different analysis of the K-Rb system using only three input parameters has been performed by Hanna, *et al.* [177].

5.3.3 ^{3}He* - ^{4}He*

In this section we briefly turn to the application of the ABM to a system of two two-electron atoms, namely the Fermi-Bose mixture of metastable helium-3 and helium-4. This system has recently been experimentally realized [39] and magnetic field tuning of the interaction parameters are of great interest. Up to now no field induced resonances have been reported experimentally nor theoretically. Based on potentials known from literature we calculate the binding energies of the least bound states and their corresponding Franck-Condon factors. Using these values as input parameters for the ABM we are able to predict Feshbach resonance positions. We use the adiabatic potential curves for the singlet ($1^1\Sigma_g^+$) and triplet ($1^3\Sigma_u^+$) potentials reported by Ref. [187] and the quintet ($1^5\Sigma_g^+$) potential we obtain from Ref. [188]. We obtain various Feshbach resonances at low magnetic field values. Two resonances of specific interest are at $B = 12.9$G in the ^{3}He* $|f = 3/2, m_f = -1/2\rangle$ ^{4}He* $|m_J = -1\rangle$ spin channel and at $B = 8.7$G in the ^{3}He* $|f = 3/2, m_f = +3/2\rangle$

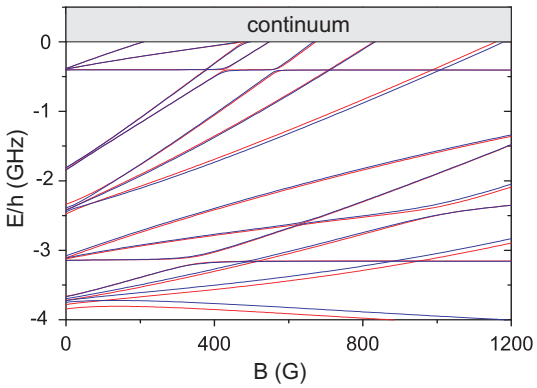

Figure 5.4: The bound state spectrum for ^{40}K-^{87}Rb for $m_F = -7/2$ plotted with respect to the threshold energy E_{thr} of the ^{40}K $|f = 9/2, m_f = -9/2 >$ + ^{87}Rb $|f = 1, m_f = +1 >$ hyperfine mixture. Red lines are ABM calculations and the blue lines are numerical coupled channels calculations. Good agreement between the two calculations is found in particular for the weakest bound levels.

^{4}He* $|m_J = 0\rangle$ spin channel. Both resonance positions are mainly determined by the accurately known quintet potential, and negligibly by the less accurately known triplet potentials. For temperatures in the ultracold regime, penning ionization collisions in the triplet potential are expected to be suppressed [189]. Spin exchange collisions of the ^{3}He* $|f = 3/2, m_f = -1/2\rangle$+^{4}He* $|m_J = -1\rangle$ $\rightarrow$^{3}He* $|f = 3/2, m_f = -3/2\rangle$+^{4}He* $|m_J = 0\rangle$ type are suppressed for ultracold samples at $B = 12.9$G because a thermal activation of $\sim 580\mu K$ is required to drive the channel. Concluding, the $B = 12.9$G resonance is a promising candidate for manipulating interspecies interactions in the ^{3}He* - ^{4}He* mixture. However, due to the large background scattering length of the ^{3}He* - ^{4}He* system, the resonances are expected to be broad. Since the resonance position shifts by an amount of the order of the resonance width (see below) the actual resonance positions might be significantly different from the stated values.

5.4 Coupling to the open channel

The model, as introduced in section 5.2, has so far been used to determine the position of the Feshbach resonances. However, a Feshbach resonance is not only characterized by its position, but also by its width. The resonance width is for a collision process inversely proportional to the lifetime of the resonance. Its value plays an important role to determine whether a Feshbach resonance can be used to explore regimes of universal physics for strongly interacting quantum gases. Wide s-wave resonances give rise to universal behavior and can be described by the scattering length only, while narrow resonances need additional parameters such as the Effective Range parameter to describe the interactions properly. For practical experimental considerations, a resonance should be sufficiently wide to allow for an accurate control over the interaction strength.
The width of a resonance is determined by the coupling between the open collision threshold channel, and the closed-channel bound state which gives rise to the Feshbach resonance

[34, 35]. This coupling is contained in the AMB, however, to make it explicit in terms of a useful matrix element, it is crucial to partition the total Hilbert space, which describes the spin and spatial degrees of freedom, into two orthogonal subspaces $\mathcal{P}$ and $\mathcal{Q}$. The open channels are located in $\mathcal{P}$ space, and the closed channels in $\mathcal{Q}$ space. Within the ABM approach we obtain the coupling between the open and closed channels without the actual use of continuum states. In Sect. 5.4.1 we present the Feshbach theory tailored to suit the ABM, we give a mathematical description of the resonant coupling, and we demonstrate from a two-channel model how the ABM bound state compares to the associated $\mathcal{P}$-space bound state, and to the dressed molecular state from which one can deduce the resonance width. In Sect. 5.4.2 we summarize the results such that the width of the Feshbach resonances can be obtained for the general multi-channel case by performing two simple basis transformations. For a more thorough treatment of the Feshbach formalism we refer the reader to [34, 35] and for its application to cold atom scattering e.g. [82].

5.4.1 Tailored Feshbach theory

By introducing the projector operators P and Q, which project onto the subspaces $\mathcal{P}$ and $\mathcal{Q}$, respectively, the two-body Schrödinger equation can be split into a set of coupled equations [82]

$$(E - \mathcal{H}_{PP})|\Psi_P\rangle = \mathcal{H}_{PQ}|\Psi_Q\rangle, \tag{5.10}$$
$$(E - \mathcal{H}_{QQ})|\Psi_Q\rangle = \mathcal{H}_{QP}|\Psi_P\rangle, \tag{5.11}$$

where $|\Psi_P\rangle \equiv P|\Psi\rangle$, $|\Psi_Q\rangle \equiv Q|\Psi\rangle$, $\mathcal{H}_{PP} \equiv P\mathcal{H}P$, $\mathcal{H}_{PQ} \equiv P\mathcal{H}Q$, etc. Within $\mathcal{Q}$ space the Hamiltonian $\mathcal{H}_{QQ}$ is diagonal with eigenstates $|\phi_Q\rangle$ corresponding to the two-body bound state with eigenvalues ϵ_Q. The energy $E = \hbar^2k^2/2\mu$ is defined with respect to the open channel dissociation threshold.
We consider one open channel and assume that near a resonance it couples to a single closed channel. This allows us to write the S matrix of the effective problem in $\mathcal{P}$ space as [82]

$$S(k) = S_P(k)\left(1 - 2\pi i\frac{|\langle\phi_Q|\mathcal{H}_{QP}|\Psi_P^+\rangle|^2}{E - \epsilon_Q - \mathcal{A}(E)}\right), \tag{5.12}$$

where $|\Psi_P^+\rangle$ are scattering eigenstates of $\mathcal{H}_{PP}$, $S_P(k)$ is the direct scattering matrix describing the scattering process in $\mathcal{P}$ space in the absence of coupling to $\mathcal{Q}$ space.
The complex energy shift $\mathcal{A}(E)$ describes the dressing of the bare bound state $|\phi_Q\rangle$ by the coupling to the $\mathcal{P}$ space and is represented by

$$\mathcal{A}(E) = \langle\phi_Q|\mathcal{H}_{QP}\frac{1}{E^+ - \mathcal{H}_{PP}}\mathcal{H}_{PQ}|\phi_Q\rangle, \tag{5.13}$$

where $E^+ = E + i\delta$ with δ approaching zero from positive values. Usually the open channel propagator $[E^+ - \mathcal{H}_{PP}]^{-1}$ is expanded to a complete set of eigenstates of $\mathcal{H}_{PP}$, where the dominant contribution comes from scattering states. To circumvent the use of scattering states we expand the propagator to Gamow resonance states, which leads to a Mittag-Leffler expansion [190]

$$\frac{1}{E^+ - \mathcal{H}_{PP}} = \frac{\mu}{\hbar^2}\sum_{n=1}^{\infty}\frac{|\Omega_n\rangle\langle\Omega_n^D|}{k_n(k - k_n)}, \tag{5.14}$$

where n runs over all poles of the S_P matrix. The Gamow state $|\Omega_n\rangle$ is an eigenstate of $\mathcal{H}_{PP}$ with eigenvalue $\epsilon_{P_n} = \hbar^2 k_n^2/(2\mu)$. Correspondingly, the dual state $|\Omega_n^D\rangle \equiv |\Omega_n\rangle^*$, is an eigenstate of $\mathcal{H}_{PP}^\dagger$ with eigenvalue $(\epsilon_{P_n})^*$. Using these dual states, the Gamow states form a biorthogonal set such that $\langle\Omega_n^D|\Omega_{n'}\rangle = \delta_{nn'}$. For bound-state poles $k_n = i\kappa_n$, where $\kappa_n > 0$, Gamow states correspond to properly normalized bound states.
We assume the scattering in the open channel is dominated by a single bound state ($k_n = i\kappa_P$). This allows us to write the direct scattering matrix in Eq. (5.12) as

$$S_P(k) = e^{-2ika_{\rm bg}} = e^{-2ika_{\rm bg}^P}\frac{\kappa_P - ik}{\kappa_P + ik} \tag{5.15}$$

where $a_{\rm bg}$ is the open channel scattering length, and the P-channel background scattering length $a_{\rm bg}^P$ is on the order of the range of the interaction potential $a_{\rm bg}^P \approx r_0$. Since we only have to consider one bound state pole (with energy $\epsilon_P = -\hbar^2\kappa_P^2/2\mu$) in $\mathcal{P}$ space, the Mittag-Leffler series Eq. (5.14) is reduced to only one term. Therefore, the complex energy shift Eq. (5.13) reduces to

$$\mathcal{A}(E) = \frac{\mu}{\hbar^2}\frac{-i\mathrm{A}}{\kappa_P(k - i\kappa_P)}. \tag{5.16}$$

where $\mathrm{A} \equiv \langle\phi_Q|\mathcal{H}_{QP}|\Omega_P\rangle\langle\Omega_P^D|\mathcal{H}_{PQ}|\phi_Q\rangle$ is a positive constant. The coupling matrix element between open-channel bound state and the closed-channel bound state responsible for the Feshbach resonance is related to A.
The complex energy shift can be decomposed into a real and imaginary part such that $\mathcal{A}(E) = \Delta_{\rm res}(E) - \frac{i}{2}\Gamma(E)$. For energies $E > 0$ the unperturbed bound state becomes a quasi-bound state: its energy undergoes a shift $\Delta_{\rm res}$ and acquires a finite width Γ. For energies below the open-channel threshold, i.e. $E < 0$, $\mathcal{A}(E)$ is purely real and $\Gamma(E) = 0$. In the low-energy limit, $k \to 0$, Eq. (5.16) reduces to

$$\mathcal{A}(E) = \Delta - iCk, \tag{5.17}$$

where C is a constant characterizing the coupling strength between $\mathcal{P}$ and $\mathcal{Q}$ space [82], given by $C = \mathrm{A}(2\kappa_P|\epsilon_P|)^{-1}$ and $\Delta = \mathrm{A}(2|\epsilon_P|)^{-1}$. Note that if the direct interaction is resonant, $|a_{\rm bg}| \gg r_0$, the energy dependence of the complex energy shift is given by [191] $\mathcal{A}(E) = \Delta - iCk(1 + ika^P)^{-1}$ where $a^P = \kappa_P^{-1}$, yielding an energy dependence of the resonance shift.
Since we consider one open channel, the (elastic) S-matrix element can be written as $e^{2i\delta(k)}$, where $\delta(k)$ is the scattering phase shift. The scattering length, defined as the limit $a \equiv -\tan\delta(k)/k$, $(k \to 0)$, is found to be

$$a(B) = a_{\rm bg}\Big(1 - \frac{\Delta B}{B - B_0}\Big), \tag{5.18}$$

which shows the well known dispersive behavior. The direct scattering process is described by the scattering length $a_{\rm bg} = a_{\rm bg}^P + a^P$. At magnetic field value B_0, where the *dressed* molecular state crosses the P-threshold, the scattering length has a singularity. Near threshold, the shifted energy of the uncoupled molecular state, $\epsilon_Q + \Delta$, can be approximated by $\Delta\mu(B - B_0)$. The field width of the resonance is found to be equal to $\Delta B = C(a_{\rm bg}\Delta\mu)^{-1}$, where $\Delta\mu$ is the magnetic moment difference of the molecular state and the P-channel atoms.

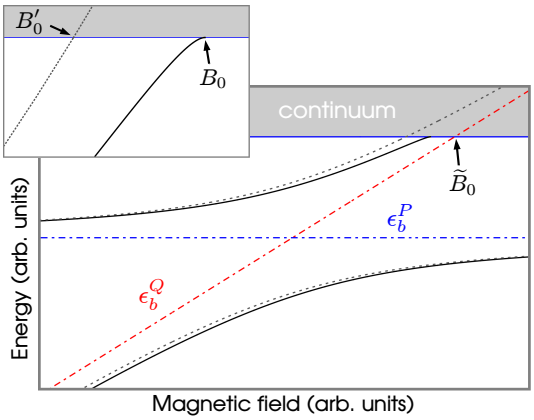

Figure 5.5: Different types of bound states, derived from a two-channel ABM model. The unperturbed molecular $\mathcal{Q}$ space bound state (dot-dashed red) is dressed by the coupling to $\mathcal{P}$ space, where ϵ_P is the uncoupled $\mathcal{P}$ space bound state (dot-dashed blue). Near threshold of the open channel (solid blue) the energy curve of the dressed molecular Feshbach state (solid black) will bend quadratically as a function of B and will cross the threshold at B_0. The uncoupled $\mathcal{Q}$ space bound state crosses the threshold at $\widetilde{B}_0$. For the original ABM bound state (gray) no threshold effects are seen and the coupled bound state crosses at B_0'.

The dressed state can be considered as a (quasi-) bound state of the total scattering system. The energy of these states is obtained by finding the poles of the total S matrix Eq. (5.12). This results in solving

$$(k - i\kappa_P)\,(E - \epsilon_Q - \mathcal{A}(E)) = 0, \tag{5.19}$$

for k. Due to the underlying assumptions, this equation is only valid for energies around threshold where the open and closed channel poles dominate.

We apply the above Feshbach theory to a (fictitious) two-channel version of ABM, and the results are shown in Fig. 5.5. This two-channel system is represented by a 2×2 Hamiltonian matrix, where there is only one open and one closed channel. The open and closed channel binding energies ϵ_P resp. ϵ_Q are given by the diagonal matrix elements, while the coupling is represented by the (identical) off-diagonal matrix elements. The closed channel bound state is made linearly dependent on the magnetic field, while the coupling is taken constant. In addition to ϵ_P and ϵ_Q, we plot the corresponding ABM solution, which in this case is equivalent to a typical two-level avoided crossing solution. The figure now nicely illustrates the evolution from ABM to the dressed ABM approach, where the latter solutions are found from the two physical solutions of Eq. (5.19), which are also plotted. Since the dressed ABM solutions account for threshold effects, they show the characteristic quadratic bending towards threshold as a function of magnetic field. From this curvature the resonance width can be deduced.

5.4.2 The dressed Asymptotic Bound state Model

To illustrate the presented model for a realistic case, we will discuss the ^{6}Li-^{40}K system prepared in the $|f_{\mathrm{Li}} m_{f_{\mathrm{Li}}}, f_{\mathrm{K}} m_{f_{\mathrm{K}}}\rangle = |1/2, +1/2, 9/2, -7/2\rangle$ two-body hyperfine state as an example throughout this section. This particular mixture is the energetically lowest spin combination of the $m_F = -3$ manifold, allowing to consider only one open channel. We note that the model can be utilized to cases containing more open channels.
In order to calculate the width of a Feshbach resonance using the method presented in Sect. 5.4.1 three quantities are required: the binding energy of the open channel ϵ_P, of the closed channel responsible for the Feshbach resonance ϵ_Q, and the coupling term between the two channels $\mathcal{H}_{PQ}$. In the following we will describe how to obtain these quantities from the ABM by two simple basis transformations.
For ultracold collisions the hyperfine and Zeeman interactions determine the threshold of the various channels and thus the partitioning of the Hilbert space into subspaces $\mathcal{P}$ and $\mathcal{Q}$, and therefore a natural basis for our tailored Feshbach formalism consists of the eigenstates of $\mathcal{H}^{\mathrm{int}}$. Experimentally a system is prepared in an eigenstate of the internal Hamiltonian $\mathcal{H}^{\mathrm{int}}$. This channel will be referred to as the entrance channel. Performing a basis transformation from the $|S m_S \mu_\alpha \mu_\beta\rangle$ states to the eigenstates of $\mathcal{H}^{\mathrm{int}}$ allows us to identify the open and closed channel subspace. The open channel has the same spin-structure as the entrance channel.
We now perform a second basis transformation which diagonalizes within $\mathcal{Q}$ space without affecting $\mathcal{P}$ space. We obtain the eigenstates of $\mathcal{H}_{QQ}$ and are able to identify the bound state responsible for a particular Feshbach resonance. The bare bound states of $\mathcal{Q}$ space are defined as $\{|\phi_{Q_1}\rangle, |\phi_{Q_2}\rangle, \ldots\}$ with binding energies $\{\epsilon_{Q_1}, \epsilon_{Q_2}, \ldots\}$. For the one dimensional $\mathcal{P}$ space, which is unaltered by this transformation, the bare bound state $|\Omega_P\rangle$ of $\mathcal{H}_{PP}$ is readily identified with binding energy ϵ_P. In the basis of eigenstates of $\mathcal{H}_{PP}$ and $\mathcal{H}_{QQ}$ we easily find the coupling matrix elements between the i-th $\mathcal{Q}$ space bound state and the open channel bound state $\langle\phi_{Q_i}|\mathcal{H}_{QP}|\Omega_P\rangle$. This gives the coupling constant $\mathrm{A_i} = \langle\phi_{Q_i}|\mathcal{H}_{QP}|\Omega_P\rangle\langle\Omega_P|\mathcal{H}_{PQ}|\phi_{Q_i}\rangle$ that determines the resonance field B_0 by solving Eq. (5.19) at threshold, which is for $E = 0$:

$$\epsilon_{Q_i}\epsilon_P = \frac{\mathrm{A_i}}{2}. \tag{5.20}$$

The field width of this Feshbach resonance is proportional to the magnetic field difference between the crossings of the dressed (B_0) and uncoupled $\mathcal{Q}$ bound states ($\widetilde{B}_0$) with threshold since

$$\Delta B = \frac{a^P}{a_{\mathrm{bg}}}(B_0 - \widetilde{B}_0) = \frac{a^P}{a_{\mathrm{bg}}}\frac{\mathrm{A_i}}{2|\epsilon_P|\Delta\mu}. \tag{5.21}$$

We illustrate the dressed ABM for Li-K in Figs. 5.6 and 5.7, for $m_F = -3$. To demonstrate the effect of $\mathcal{H}_{PQ}$, we plotted for comparison both the uncoupled and dressed bound states [3]. Details of near-threshold behavior (gray shaded area in Fig. 5.6) are shown in Fig. 5.7 together with the obtained scattering length. We solved the pole equation of the total S-matrix Eq. (5.19) for each Q-state and plotted only the physical solutions which cause Feshbach resonances. The dressed bound states show the characteristic quadratic bending near the threshold. We have used C_6 to determine r_0 ($\approx a^P_{\mathrm{bg}}$) from Eq. 5.8.
Table 5.1 summarizes the results of the dressed ABM for the Li-K mixture. Note that the position of the Feshbach resonances will be slightly different compared to the results from

[3] For clarity only one of the two physical solutions is shown.

Table 5.1: The positions of experimentally observed s-wave Feshbach resonances of ^{6}Li$-^{40}$K. Column 2 gives the ^{6}Li ($m_{f_{Li}}$) and ^{40}K (m_{f_K}) hyperfine states. For all resonances $f_{Li} = 1/2$ and $f_K = 9/2$. Note that the experimental width of the loss feature $\Delta B_{\rm exp}$ is not the same as the field width ΔB of the scattering length singularity. Feshbach resonance positions B_0 and widths ΔB for ^{6}Li-^{40}K as obtained by the dressed ABM, obtained by minimizing χ^2. The last two columns show the results of full coupled channels (CC) calculations. All magnetic fields are given in (G). The experimental and CC values for $m_F < 0$ and $m_F > 0$ are taken from Ref. [17] and [18] respectively.

		Experiment		dressed ABM		CC	
m_F	$m_{f_{Li}}$,m_{f_K}	B_0	$\Delta B_{\rm exp}$	B_0	ΔB	B_0	ΔB
-5	$-\frac{1}{2}, -\frac{9}{2}$	215.6	1.7	216.2	0.16	215.6	0.25
-4	$+\frac{1}{2}, -\frac{9}{2}$	157.6	1.7	157.6	0.08	158.2	0.15
-4	$+\frac{1}{2}, -\frac{9}{2}$	168.2	1.2	168.5	0.08	168.2	0.10
-3	$+\frac{1}{2}, -\frac{7}{2}$	149.2	1.2	149.1	0.12	150.2	0.28
-3	$+\frac{1}{2}, -\frac{7}{2}$	159.5	1.7	159.7	0.31	159.6	0.45
-3	$+\frac{1}{2}, -\frac{7}{2}$	165.9	0.6	165.9	0.0002	165.9	0.001
-2	$+\frac{1}{2}, -\frac{5}{2}$	141.7	1.4	141.4	0.12	143.0	0.36
-2	$+\frac{1}{2}, -\frac{5}{2}$	154.9	2.0	154.8	0.50	155.1	0.81
-2	$+\frac{1}{2}, -\frac{5}{2}$	162.7	1.7	162.6	0.07	162.9	0.60
+5	$+\frac{1}{2}, +\frac{9}{2}$	114.47(5)	1.5(5)	115.9	0.91	114.78	1.82

the regular ABM, for equal values of $\epsilon_S^{\nu,0}$. Therefore, we have again preformed a χ^2 analysis and we found new values of the binding energies $\epsilon_0 = 713$[MHz] and $\epsilon_1 = 425$[MHz], which yields a lower χ^2 minimum as compared to the ABM calculation.
The obtained value of ΔB generally underestimates the field width of a resonance. This originates from the fact that only the dominant bound state pole corresponding to a^P has been taken into account. By including the pole of the dominant *virtual* state in the Mittag-Leffler expansion, ΔB will increase, and the value of a_{bg} will become more accurate.

5.5 Summary and Conclusion

We developed a novel method to describe Feshbach resonances. The model allows for fast and accurate prediction of resonance positions and widths with very little experimental input. The combination of the ABM with the accumulated phase allows to describe Feshbach resonances for a very large number of systems. We have demonstrated the application on three very different systems. The model underestimates the resonance width because we have neglected the dominant virtual state contribution in the Mittag-Leffler expansion. A further improvement of the model would be to take the virtual states into account. With this work we demonstrate that by performing simple matrix operations Feshbach resonances can be accurately described, allowing for a broad application for experiments working with ultracold gases.

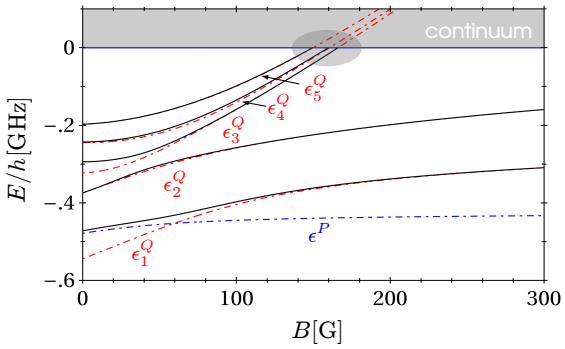

Figure 5.6: Dressed molecular states for Li-K for $m_F = -3$ (black lines, see also Table 5.1). The uncoupled $\mathcal{Q}$ and $\mathcal{P}$ bound states ($\mathcal{H}_{PQ} = 0$) are represented by the dot-dashed lines (red and blue respectively), indicating the effect of the $\mathcal{H}_{PQ}$ coupling.

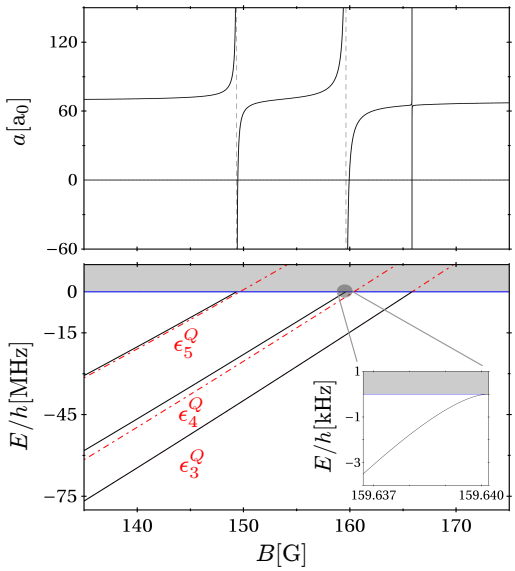

Figure 5.7: The dressed molecular states are shown near threshold (black). The field width of a resonance is related to the magnetic field difference of where the dressed and uncoupled $\mathcal{Q}$ bound state cross the threshold.